

**Membrane-anchored serine protease matriptase is a trigger of pulmonary fibrogenesis**

Olivier Bardou<sup>1,2</sup> §, Awen Menou<sup>1,2</sup> §, Charlène François<sup>1,2</sup>, Jan Willem Duitman<sup>3</sup>, Jan H. von der Thüsen<sup>4</sup>, Raphaël Borie<sup>2,5</sup>, Katiuchia Uzzun Sales<sup>6,7</sup>, Kathrin Mutze<sup>8</sup>, Yves Castier<sup>9</sup>, Edouard Sage<sup>10</sup>, Ligong Liu<sup>11</sup>, Thomas H. Bugge<sup>6</sup>, David P. Fairlie<sup>11</sup>, Mélanie Königshoff<sup>8</sup>, Bruno Crestani<sup>1,2,5#</sup>, Keren S. Borensztajn<sup>1,2#\*</sup>

<sup>1</sup>Inserm UMR1152, Medical School Xavier Bichat, 75018, Paris, France

<sup>2</sup>Université Paris Diderot, Sorbonne Paris Cité, Département Hospitalo-universitaire FIRE (Fibrosis, Inflammation and Remodeling) and LabEx Inflammex, Paris, France

<sup>3</sup>Center for Experimental and Molecular Medicine, Academic Medical Center, Amsterdam, The Netherlands

<sup>4</sup>Department of Pathology, Erasmus Medical Centre, Rotterdam, The Netherlands

<sup>5</sup>Assistance Publique-Hôpitaux de Paris, Department of Pulmonology A, Competence Center for rare lung diseases, Bichat-Claude Bernard University Hospital, 75018, Paris, France

<sup>6</sup>Oral and Pharyngeal Cancer Branch National Institute of Dental and Craniofacial Research, National Institutes of Health Bethesda, MD, USA.

<sup>7</sup>Department of Cell and Molecular Biology Ribeirão Preto School of Medicine University of São Paulo Ribeirão Preto, SP, Brazil.

<sup>8</sup>Member of the German Center of Lung Research, Comprehensive Pneumology Center, University Hospital, Ludwig-Maximilians University, Helmholtz Zentrum München, Munich, Germany

<sup>9</sup>Assistance Publique-Hôpitaux de Paris, Department of Vascular and Thoracic Surgery, Bichat-Claude Bernard University Hospital, Denis Diderot University and Medical School Paris VII, France

<sup>10</sup>Department of Thoracic Surgery and Lung Transplantation, Hôpital Foch, Suresnes, France

<sup>11</sup>Institute for Molecular Bioscience, University of Queensland, Brisbane, Qld 4072, Australia

\*To whom correspondence should be addressed. E-mail : keren.borensztajn@inserm.fr, phone +33 1 57 27 75 85, Fax : +33 1 57 27 75 51

§ These authors contributed equally to the work

# These authors contributed equally to the work

**Running title:** Matriptase in Idiopathic Pulmonary Fibrosis

**Keywords:** Idiopathic Pulmonary Fibrosis, fibroblast, Matriptase, protease-activated receptor-2, bleomycin, camostat mesilate

Word count: 3497 words

This article has an online data supplement, which is accessible from this issue's table of content online at [www.atsjournals.org](http://www.atsjournals.org)

Abstract word count: 248 words

**Authors contribution:** Conception and design: OB, AM, KB, BC; Analysis and interpretation: CF, AM, JvdT, RB, KS, ES, YC, LL, TB, DF, MK; Drafting the manuscript for important intellectual content: OB, AM, KB, BC.

**Grants and financial support:** OB, AM and KB were supported by grants from the Fondation pour la Recherche Medicale AJE201121 to KB and Agence Nationale pour la Recherche ANR-14-CE15-0010-01. JWD was supported by a grant from Dutch Lung Foundation, number: 9.2.14.085FE KM and MK were supported by grants from the Helmholtz Association. LL and DF were supported by NHMRC grant 1047759 and Senior Principal Research Fellowship to DF (1027369). TB and KS were supported by from the NIDCR Intramural Research Program.

## AT A GLANCE COMMENTARY

### Scientific Knowledge on the Subject

Idiopathic Pulmonary fibrosis (IPF) is characterized by the deposition of excessive extracellular matrix and the destruction of lung parenchyma, resulting from an aberrant wound healing response. Although IPF is often associated with an imbalance in protease activity, the mechanisms underlying the sustained repair mechanisms are not fully understood.

### What This Study Adds to the Field

We showed that the recently identified membrane-anchored serine protease matriptase is upregulated in IPF in humans and during pulmonary fibrogenesis in mice. Matriptase triggers fibroproliferative responses in pulmonary cells via Protease-Activated Receptor-2 activation. In an experimental mouse model, lung injury and fibrosis were reduced through matriptase depletion, using either the pharmacological inhibitor camostat mesilate (already in clinical use for other diseases), or by genetic down-regulation by using matriptase hypomorphic mice, that have a 93%-fold reduction in lung matriptase mRNA levels. These data indicate that matriptase is influential in promoting pulmonary fibrogenesis *in vivo*, and show that camostat mesilate is a potential treatment for IPF.

## Abstract

*Rationale:* Idiopathic Pulmonary fibrosis (IPF) is a devastating disease, which remains refractory to current therapies.

*Objectives:* To characterize the expression and activity of the membrane-anchored serine protease matriptase in IPF in humans and unravel its potential role in human and experimental pulmonary fibrogenesis.

*Methods:* Matriptase expression was assessed in tissue specimens from IPF patients versus controls using qRT-PCR, immunohistochemistry and Western blotting, while matriptase activity was monitored by fluorogenic substrate cleavage. Matriptase-induced fibroproliferative responses and the receptor involved were characterized in human primary pulmonary fibroblasts by Western blot, viability and migration assays. In the murine model of bleomycin-induced pulmonary fibrosis, the consequences of matriptase depletion, either by using the pharmacological inhibitor camostat mesilate, or by genetic down regulation using matriptase hypomorphic mice, were characterized by quantification of secreted collagen and immunostainings.

*Measurements and Main Results:* Matriptase expression and activity were upregulated in IPF and bleomycin-induced pulmonary fibrosis. In cultured human pulmonary fibroblasts, matriptase expression was significantly induced by TGF- $\beta$ . Further, matriptase elicited signaling via Protease-Activated Receptor-2 (PAR-2), and promoted fibroblast activation, proliferation and migration. In the experimental bleomycin model, matriptase depletion, by the pharmacological inhibitor camostat mesilate or by genetic down-regulation, diminished lung injury, collagen production and TGF- $\beta$  expression and signaling.

*Conclusions:* These results implicate increased matriptase expression and activity in the pathogenesis of pulmonary fibrosis in human IPF and in an experimental mouse model. Overall, targeting matriptase, or treatment by camostat mesilate, which is already in clinical use for other diseases, may represent potential therapies for IPF.

## Introduction

Idiopathic pulmonary fibrosis (IPF) is a devastating chronic fibrotic lung disease with a median survival of 2-3 year [1]. Options for the treatment of IPF are limited. Only two drugs, Pirfenidone and nintedanib, have demonstrated efficacy in slowing fibrosis progression in patients with mild to moderate IPF [2, 3]. Therefore, novel treatment options are sorely needed. The current paradigm on the underlying pathogenic mechanisms postulates that IPF is an “epithelial-fibroblastic disease”, *i.e.* a fibroproliferative disorder preceded by alveolar epithelial injury and activation, with fibrotic foci representing the primary sites of injury and aberrant repair [1]. The precise signals triggering the aberrant and sustained wound healing response in IPF remain elusive, and represent an area of intense investigation. Evidence for diffuse infiltration of immune cells in the fibrotic lung also strongly suggest that auto-immunity plays a role in the course of the disease. Accordingly, immunomodulatory therapies are currently being evaluated in early-phase clinical trials [4, 5].

Matriptase belongs to the recently identified Type II-transmembrane serine protease family [6]. Membrane anchorage enables matriptase to initiate pericellular proteolysis in the microenvironment, and to interact with vicinal membrane proteins on the same cell surface and/or on neighbouring cells. Matriptase activity is regulated by hepatocyte growth factor activator inhibitor type (HAI)-1, through formation of a stoichiometric 1:1 complex. Over the last decade, compelling evidence has demonstrated that matriptase deregulation is influential in a broad variety of pathological processes, including cancer and skin diseases [6, 7]. Three major macromolecular substrates of matriptase have been identified: hepatocyte growth factor, Protease-activated receptor-2 and urokinase-type plasminogen activator [6]. Through the cleavage of these substrates, matriptase triggers specific responses including cell proliferation, migration, inflammatory cytokine production, inflammatory cell recruitment, hyperplasia and fibrosis [8, 9]. These responses are crucial in fibrotic diseases [10, 11], but the role of matriptase in fibrotic disorders has thus far never been explored.

We recently established a link between Protease-activated receptor(PAR)-2 and pulmonary fibrosis progression in humans and mice [12]. PAR-2 belongs to the G-protein-coupled receptor superfamily. Its activation by proteolytic cleavage triggers multiple cell signaling pathways, the functional consequences of which are crucial in pathologies such as aberrant wound repair mechanisms [13]. However, the relevant PAR-2 agonists involved in

IPF remain unknown. Considering that matriptase is expressed physiologically in murine and human lung [14], orchestrates tissue remodelling through its potent trypsin-like activity and is able to activate PAR-2, in the present study, we explore whether matriptase is implicated in the progression of human and experimental pulmonary fibrosis.

## **Materials and Methods**

Methodology for the murine bleomycin model, collagen quantification, qRT-PCR, cell culture studies, histology and immunohistochemistry can be found in the online supplement.

### **Human Tissues**

Lung tissue was obtained from 61 patients with IPF (8 females, 53 males; mean age  $57.6 \pm 7.5$  years), and 43 control subjects (patients undergoing lung surgery for removal of a primary lung tumor; mean age  $62.5 \pm 13.8$ , 17 females, 26 males). Control tissues were obtained from noninvolved segment, remote from the solitary tumor lesion, and normalcy of control lungs was verified histologically as described previously [15, 16]. Primary fibroblasts were isolated as described in [15]. The study protocol was approved by the institutional Ethics committee (comité d'éthique du CEERB Paris Nord, biobank registration number DC 2009-940). Details for isolation of AECs and fibroblasts from the German cohort are provided in the supplementary methods section.

### **Animals**

C57BL/6N mice were from Janvier Labs (Le Genest Saint Isle, France). When indicated, 0.5 mg camostat mesilate (CM) treatment was initiated 7 days after bleomycin challenge. CM was administered intranasally every other day from day 7-14. Matriptase hypomorphic mice have been described previously [17]. Briefly, these mice possess one null allele and one allele in which a reporter gene trap is inserted into the matriptase locus and disrupts gene expression. A low level of alternative splicing in the gene trap allele results in low level synthesis of full length matriptase, which is sufficient to enable mouse survival. Experiments with matriptase hypomorphic mice were littermate controlled from mice generated from heterozygous crosses [18]. The bleomycin murine model of pulmonary fibrosis was set up as described previously [19]. Additional details are provided in the online supplement.

## Statistical Analyses

Statistical analyses were conducted using GraphPad Prism (GraphPad Software, San Diego, CA). Data are expressed as mean  $\pm$  SEM. Comparisons between two groups were analyzed using two-tailed unpaired t-tests when the data were normally distributed, otherwise Mann-Whitney analysis was performed. P values of  $<0.05$  were considered to indicate a statistically significant difference.

## Results

### *Increased matriptase expression and activity in the lungs of IPF patients*

We first investigated whether the expression and activity of matriptase are deregulated in IPF. The mRNA levels of matriptase were determined in human lung tissue specimen from controls and IPF patients using qRT-PCR. As shown in Table I and Figure 1A, in IPF tissues, matriptase mRNA was significantly upregulated (by  $1.6\pm 0.1$ -fold) compared to control. We confirmed matriptase upregulation by immunoblotting. As shown in Figure 1B, in control lungs (lanes 1-6), matriptase expression is low, and increased by 2.25 fold in IPF lungs (lanes 8-12). Additionally, consistent with previous studies [20, 21], PAR-2 expression was upregulated in IPF lung ( $3.5\pm 2$ -fold) (Figure 1B). Subsequently, we determined the proteolytic activity of matriptase in control and IPF tissues by monitoring the cleavage of its highly specific fluorogenic peptide substrate t-butyloxycarbonyl Boc-Gln-Ala-Arg-MCA (Boc-QAR-AMC) [7, 22]. Figure 1C shows that the proteolytic activity significantly increased ( $206\pm 65\%$ ) in IPF lungs compared to controls. Consistently, increased matriptase antigen level and activity were detected in BALF IPF patients (Supplemental Figure E1).

Deregulation of matriptase activity often relates to an imbalance with its endogenous inhibitor HAI-1. Hence, we determined the HAI-1 mRNA levels by qPCR and determined the ratio of matriptase/HAI-1 mRNA expression in control versus IPF lungs, as previously described [23]. In IPF tissues, we observed a 1.2-fold increase in HAI-1 mRNA, and the ratio matriptase/HAI-1 was slightly upregulated in IPF patients (Table 1).

Next, we examined the cellular distribution of matriptase in lung biopsies of IPF patients. Immunohistochemical staining showed prominent matriptase immunoreactivity, in macrophages and epithelial cells overlying fibroblast foci, and a weaker staining in (myo)fibroblasts of these foci (Figure 1D-I). Endothelium staining was even weaker (not

shown). In contrast, only sparse staining of alveolar type II cells (AECs) and monocytes was observed in the nonfibrotic part of the lung of these patients (Figure 1J). There was no detectable signal for similar sections stained with an isotype-specific control antibody (Figure 1K). Finally, using primary IPF AEC and fibroblasts derived from a different (German) cohort, we assessed the relative expression of matriptase by qPCR and confirmed that matriptase mRNA level is higher in fibrotic AECs, and weaker in fibrotic fibroblasts (Figure 1L).

### ***Modulation of matriptase expression in vitro in pulmonary cells***

We next analysed the modulation of matriptase expression in pulmonary cells. Western blots of primary human pulmonary fibroblasts derived from IPF tissues (figure 2A) showed 1.7±0.4-fold higher matriptase expression (lanes 6-9) than from control fibroblasts (lanes 1-5). Since TGF-β is a master switch in the development of fibrosis during IPF [24], we also assessed its action on pulmonary cells. Stimulation of control (lanes 10-14) or fibrotic (lanes 15-18) fibroblasts for 48h by TGF-β (1ng/mL) robustly enhanced matriptase expression by 3.1±0.5 and 5.1±1.5-fold respectively (Figure 2A). Consistent with previous studies [20, 21], PAR-2 was upregulated in IPF and TGF-β-stimulated control fibroblasts (by 2.4±0.8- and 4.5±0.8-fold respectively). To our knowledge, the action of TGF-β on PAR-2 expression in IPF fibroblasts has never been assessed. We observed in TGF-β-stimulated IPF fibroblasts that PAR-2 expression was unchanged (p=0.057) (Figure 2A). The effects of TGF-β on matriptase expression were also examined in epithelial pulmonary cells and in Normal Human Lung Fibroblasts (NHLF). TGF-β induced matriptase upregulation by 4.5±1-fold in NHLF (Figure 2B) and by 1.6±0.3-fold in epithelial pulmonary cells (Figure 2D, lanes 1-3). We also assessed the effects of matriptase on its own expression. We observed that, while 48h stimulation with 0-10nM recombinant matriptase (which displays a potent activity similar to endogenous matriptase [7]) had no effect on fibroblasts (Figure 2C), matriptase efficiently upregulated its own expression in epithelial pulmonary cells at 1 and 10nM (by 1.9±0.3- and 2.3±0.2-fold respectively) (Figure 2D, lanes 4-5)

### ***Matriptase evokes fibroproliferative responses in vitro via PAR-2 activation***

We next characterized the signalling elicited by matriptase in pulmonary cells. Control fibroblasts were stimulated for 30 minutes with 0-10 nM matriptase, or for 0-60 minutes with 1nM matriptase. We analyzed the phosphorylation of ERK1/2 and Akt, which mediate

influential signaling pathways in pulmonary fibrogenesis [25]. Figure 3A shows that matriptase stimulated a time- and dose-dependent phosphorylation of both kinases. Furthermore, to determine whether PAR-2 mediates matriptase-induced signalling, cells were preincubated for 30 minutes with the PAR-2 blocking antibody, SAM-11 [26, 27], and subsequently stimulated for 10 min with 1nM matriptase. Pretreatment with SAM-11 strongly reduced the matriptase-induced phosphorylation of ERK1/2 or Akt (Figure 3A). Similar results were obtained with epithelial pulmonary cells (Figure 3B) and NHLF (not shown). Altogether, these data demonstrate that matriptase signals to pulmonary cells via PAR-2 activation.

The effects of 48h incubation with 0-10nM matriptase on cell proliferation were also assessed by a WST-1 assay. As shown in figure 3C, 1nM and 10nM matriptase significantly enhanced control fibroblast proliferation by  $188\pm134\%$  and  $239\pm79\%$  respectively. Similar results were obtained with NHLF. Further, matriptase-induced cell survival was PAR-2 dependent as pretreatment with  $10\ \mu\text{M}$  GB88, a specific PAR-2 antagonist [28], abolished the effect of 10 nM matriptase on fibroblast proliferation. Strikingly, matriptase led to a dose-dependent decrease in epithelial pulmonary cell proliferation by  $19.4\pm1.1\%$  (Figure 3D). We also analyzed the effects of matriptase on fibroblast migration in a modified Boyden chamber. As shown on Figure 3E, 1nM matriptase enhanced cell migration by  $175\pm46\%$ . This effect was reversed by  $10\ \mu\text{M}$  GB-88, underlying PAR-2 involvement in matriptase-mediated cell migration. We subsequently examined whether matriptase triggers fibroblast activation, and stimulate ECM component synthesis. As shown in Figure 3F, 48h stimulation with 1 or 10 nM matriptase promoted significant increases ( $1.5\pm0.3$ - and  $3.1\pm1.2$ -fold) in  $\alpha$ -SMA, a hallmark for myofibroblast differentiation, as well as in production of collagen ( $1.6\pm0.3$ - and  $2.4\pm0.6$ -fold) and fibronectin (by  $1.9\pm0.7$ - and  $2.3\pm0.7$ -fold). These responses were specific and PAR-2 dependent. Preincubation of the cells for 1h with  $5\ \mu\text{M}$  camostat mesilate (CM), a specific, potent matriptase inhibitor [29-31], which does not affect thrombin activity (Supplementary Figure E3), or the PAR-2 antagonist GB88 ( $10\ \mu\text{M}$ ), reversed matriptase-induced protein expression (Figure 3G).

Overall, these data implicate a contributing role for matriptase in IPF pathogenesis, prompting us to further analyse the effects of modulating matriptase in experimental bleomycin-induced pulmonary fibrosis.

### ***Matriptase expression and activity are increased during experimental pulmonary fibrosis***

Mice subjected to a single orotracheal instillation of bleomycin developed pulmonary fibrosis over a 2-week time course (inflammatory phase: day 1-7, fibrosing phase day 7-14). Figure 4A shows data for the temporal modulation of matriptase expression and activity in murine lungs in this experimental model. Matriptase activity significantly increased by day 7 (by  $388\pm 114\%$ ) and day 14 (by  $587\pm 50\%$ ) (Figure 4A, top panel). Accordingly, immunoblotting confirmed an increase in pulmonary matriptase expression 14 days after bleomycin instillation (Figure 4A, bottom panel). Hence, we assessed the efficacy of the matriptase inhibitor camostat mesilate (CM), when administrated from day 7 onwards after the bleomycin challenge (delayed treatment), on pulmonary fibrosis development.

### ***Inhibition of matriptase by camostat mesilate attenuates pulmonary fibrogenesis in vivo***

CM is clinically used to treat pancreatitis. We initiated a delayed treatment by CM at the same dose range administered to patients [32]. CM treatment significantly reduced matriptase activity in murine lung homogenates 14 days after bleomycin challenge ( $853\pm 130\%$  to  $381\pm 63\%$ ) (Figure 4B). Additionally, the loss in body weight (determined from day 7 onwards) in the bleomycin group was significantly attenuated in the CM-treated group (Figure 4C). We next quantified total pulmonary collagen content 14 days after bleomycin challenge. The collagen content strongly increased after bleomycin treatment (from  $1261\pm 463$  to  $2408\pm 747$   $\mu\text{g/g}$  lung), and was blunted in the bleomycin+CM group ( $1527\pm 664$   $\mu\text{g/g}$  lung) (Figure 4D). Accordingly, histologic assessment of the lung structure revealed that delayed CM treatment significantly attenuated the alveolar wall thickening due to inflammation and fibrosis (Figure 4E, bottom panels). The Ashcroft scoring system confirmed that CM treatment significantly reduced the severity of the lesions induced by bleomycin exposure ( $2.7\pm 0.3$  versus  $4.9\pm 0.2$ , respectively) (Figure 4F). Accordingly, a reduced fibrosis score determined on semi-quantitative assessment of Masson's trichrome staining was observed in CM-treated animals (Figure 4G). A potential mechanism by which matriptase inhibition is protective could be by preventing myofibroblast differentiation. Indeed, semi-quantitative assessment of  $\alpha$ -SMA staining revealed a markedly reduced  $\alpha$ -SMA expression in bleomycin+CM versus bleomycin groups ( $1.3\pm 0.7$  versus  $3.61\pm 0.1$ , Figure 4H). We next assessed TGF- $\beta$  expression and signaling. As shown in Figure 4I, TGF- $\beta$  mRNA

was strongly upregulated upon bleomycin challenge (by  $177\pm 50\%$ ), while in the bleomycin+CM-treated group, it was significantly reduced. Accordingly, Smad-2 phosphorylation was significantly increased by bleomycin, and was markedly attenuated by CM (respectively  $2.1\pm 0.7$ - versus  $1.2\pm 0.4$ -fold increase).

Finally, we determined the effects of CM on the inflammatory response. The total number of macrophages in BALF was increased by bleomycin, but remained unchanged in the CM-treated group (Figure 4J). The levels of the cytokines TNF- $\alpha$ , IL-6, and MCP-1 were also unaffected by CM treatment (data not shown). Thus, CM does not seem to modulate the inflammatory responses. Altogether, these data suggest that CM treatment affords protection from bleomycin-induced pulmonary fibrosis, with the prevailing mechanisms seeming to be antifibrotic rather than anti-inflammatory.

### ***Consequences of matriptase genetic down-regulation in experimental pulmonary fibrogenesis***

Finally, we assessed the effects of genetic matriptase depletion in pulmonary fibrosis. Matriptase deficiency is lethal [33]. Hence, we used matriptase hypomorphic mice, which express low levels of pulmonary matriptase [17]. Indeed, we observed that Matriptase hypomorphic mice expressed  $7.1\pm 6\%$  of the matriptase mRNA levels detected in lung tissues of littermate control mice (Figure 5A). Matriptase hypomorphic mice and controls were subjected to bleomycin-induced pulmonary fibrosis and sacrificed 14 days after bleomycin challenge. Quantification of total pulmonary collagen content in controls revealed that collagen was significantly increased after bleomycin treatment (from  $1232\pm 342$  to  $2049\pm 569$   $\mu\text{g/g}$  lung). Interestingly, in the hypomorphic mice, there was no significant difference in collagen content between the saline- or bleomycin-treated groups ( $1369\pm 286$  versus  $1070\pm 462$   $\mu\text{g/g}$  lung) (Figure 5B). Histologic assessment of the lung structure revealed that in matriptase hypomorphic mice, bleomycin-induced lung injury was reduced compared to the controls (Figure 5C). Indeed, the severity of the lesions was reduced on the Ashcroft scale ( $2.7\pm 1$  versus  $5\pm 1$  respectively, Figure 5D). Quantitative assessment of  $\alpha$ -SMA staining demonstrated that, after bleomycin treatment,  $\alpha$ -SMA expression was significantly reduced in matriptase hypomorphic mice compared to controls (Figure 5E). Finally, analysis of TGF- $\beta$  expression and signaling in the two groups of mice revealed that, again, bleomycin elicited a significant increase of TGF- $\beta$  mRNA in the control mice. In matriptase hypomorphic mice, there was no significant difference between saline and bleomycin groups. Accordingly, Smad-

2 phosphorylation was increased by bleomycin in control, but not in hypomorphic mice (respectively by  $2.5\pm 0.8$  versus  $1.4\pm 0.5$ -fold; Figure 5F)

Hence, genetic matriptase down-regulation inhibits the bleomycin-induced collagen secretion, lung injury and  $\alpha$ -SMA expression with an efficiency comparable to that of pharmacological inhibition with camostat mesilate.

## Discussion

The present study establishes for the first time a link between the membrane-anchored serine protease matriptase and IPF. Increased matriptase expression and activity were detected in human IPF specimen compared to controls. *In vitro*, we observed in pulmonary cells a remarkable plasticity in matriptase expression in response to TGF- $\beta$ . Of note, the fibroblastic modulation of PAR-2 is akin of that observed for matriptase. PAR-2 is a major matriptase substrate [6], and is involved in IPF [12, 21, 34, 35]. Indeed, we observed that matriptase triggers key features involved in IPF via PAR-2 activation. Strikingly, matriptase orchestrates fibroblast activation (characterized by proliferation, migration, differentiation and protein synthesis) while it contributes to pulmonary epithelial cell loss. Because membrane-anchorage enables matriptase to interact with vicinal proteins on the same cell surface or on neighbor cells, it may be hypothesized that epithelial and/or fibroblastic matriptase contribute to the aberrant epithelial-mesenchymal crosstalk characterizing IPF, eventually leading to sustained pathological wound healing response. Accordingly, in our experimental model of bleomycin-induced pulmonary fibrosis, matriptase genetic down-regulation effectively limits fibrosis development, collagen deposition, myofibroblast activation, TGF- $\beta$  expression and signaling, thereby establishing a causal role for matriptase in pulmonary fibrosis pathogenesis.

We showed that, similar to the results obtained with matriptase hypomorphic mice, delayed CM treatment (*i.e.* initiated after the inflammatory phase of the model, 7 days after the bleomycin challenge) substantially reduces pulmonary fibrosis. CM has successfully been used in experimental models of liver, pancreatic and renal fibrosis [36-38], and the antifibrogenic effect of CM were attributable (at least partly) to reduced TGF- $\beta$  expression and signaling. So far, CM efficiency had never been assessed in pulmonary fibrosis, and our results are consistent with these findings. CM has a relatively narrow inhibition spectrum

among serine proteases. Indeed, besides matriptase, it displays a very high specificity for trypsin, and, to a lower extent, prostasin [29, 31], the expressions of which were unchanged in IPF lungs (data not shown). Because CM is already used in clinics, its safety and tolerance are well established [31, 32]. All these advantages would be particularly favorable for long-term treatment in IPF patients.

Several issues are relevant to interpreting these data. First, one might hypothesize that the CM effects may be mediated through thrombin inhibition. However, we demonstrated comparable antifibrotic effects of genetic and pharmacological matriptase depletion. Furthermore, *in vitro*, thrombin activity is unaffected by a dose of CM which completely inhibits matriptase activity (Supplementary Figure E3). Nevertheless, a possible involvement of other unknown serine protease(s) that is/are inhibited by CM in the pathogenesis of IPF cannot be excluded. Second, the antifibrotic effects of CM might be due to direct bleomycin inhibition. However, CM treatment in the present study was delayed, and so is unlikely to interfere with the course of events triggered by bleomycin immediately after its delivery. Moreover, CM is efficient in the abovementioned experimental models of fibrosis affecting other organs, where fibrosis was induced by the administration of different agents [36, 37, 39, 40], surgical procedures [38, 41], or even spontaneously [42]. Third, the collagen content might be overestimated in the Sircol assay [43]. However, the data are consistent with Ashcroft, masson's trichrome and  $\alpha$ -SMA scoring in the different experimental conditions.

In the present study, matriptase was upregulated by  $\sim 1.56$ -fold in IPF. Interestingly, another study demonstrated that, in mice, a modest overexpression (1.2- to 1.4-fold) of matriptase in the skin was sufficient to cause spontaneous squamous cell carcinoma in the absence of other environmental or genetic challenges, and dramatically potentiated carcinogen-induced tumor formation. Regulation of matriptase activity by HAI-1 overexpression negated the oncogenic effects of matriptase [44]. These observations are consistent with the results of our study. We find that a modest increase in matriptase expression and activity is associated with pulmonary fibrogenesis, and matriptase depletion, either using camostat mesilate, or genetic down-regulation, ablates this phenotype. Additionally, the reported matriptase-induced malignant conversion was preceded by progressive dermal hyperplasia and fibrosis, observations that are striking in the context of IPF. Indeed, the incidence of lung cancer in patients with IPF is higher than the general population [45]. Thus, it is tempting to speculate that a modest overexpression of matriptase in human lung contributes to higher tumor susceptibility, but the identification of the specific

molecular events that enable matriptase-induced transformation in the lung remains a substantial challenge.

To our knowledge, this is the first report for matriptase expression and modulation during pathogenesis in human pulmonary fibroblasts. Noteworthy, in the fibroblastic foci of IPF lungs, fibroblast staining for matriptase was weaker than in overlying epithelium. Moreover, in line with heterogeneity of the fibroblast population [46], not all fibroblasts were positive for matriptase. Nevertheless, our *in vitro* data confirmed that matriptase expression is increased in primary IPF fibroblasts compared to controls, and strongly driven by TGF- $\beta$  in control fibroblasts. Obviously, TGF- $\beta$  is not the sole cytokine contributing to fibrogenesis, and multiple factors and pathways involved in IPF pathogenesis [47] may also impact on matriptase expression. While matriptase expression and functions were initially ascribed to epithelial cells, recent studies demonstrated that matriptase is expressed in diverse cell types including normal and malignant mesenchymal cells [48-52]. Together with the present study, this shows the remarkable plasticity of matriptase in response to different stimuli, raising important new questions. It would be important to determine whether matriptase is salient in other diffuse parenchymal lung diseases, where CM might also be effective. The role of matriptase on AECII is obviously of interest in these future studies. Furthermore, CM is efficient in experimental models of fibrosis affecting other organs where PAR-2 is instrumental [40, 53, 54]. Thus, further studies aimed at elucidating the role of matriptase in these diseases are warranted.

In conclusion, our results reveal a new role for matriptase in IPF, and indicate that targeting matriptase, or treatment by CM, which is already in clinical use for other diseases, may represent potential therapies for the treatment of IPF.

## References

1. King, T.E., Jr., A. Pardo, and M. Selman, *Idiopathic pulmonary fibrosis*. *Lancet*, 2011. **378**(9807): p. 1949-61.
2. King, T.E., Jr., et al., *A phase 3 trial of pirfenidone in patients with idiopathic pulmonary fibrosis*. *N Engl J Med*, 2014. **370**(22): p. 2083-92.
3. Richeldi, L., et al., *Efficacy and safety of nintedanib in idiopathic pulmonary fibrosis*. *N Engl J Med*, 2014. **370**(22): p. 2071-82.
4. Taille, C., et al., *Identification of periplakin as a new target for autoreactivity in idiopathic pulmonary fibrosis*. *Am J Respir Crit Care Med*, 2011. **183**(6): p. 759-66.
5. Wuyts, W.A., et al., *Combination therapy: the future of management for idiopathic pulmonary fibrosis?* *Lancet Respir Med*, 2014. **2**(11): p. 933-42.
6. Szabo, R. and T.H. Bugge, *Membrane-anchored serine proteases in vertebrate cell and developmental biology*. *Annu Rev Cell Dev Biol*, 2011. **27**: p. 213-35.
7. Sales, K.U., et al., *Matriptase initiates activation of epidermal pro-kallikrein and disease onset in a mouse model of Netherton syndrome*. *Nat Genet*, 2010. **42**(8): p. 676-83.
8. Szabo, R., et al., *c-Met-induced epithelial carcinogenesis is initiated by the serine protease matriptase*. *Oncogene*, 2011. **30**(17): p. 2003-16.
9. Sales, K.U., et al., *Non-hematopoietic PAR-2 is essential for matriptase-driven pre-malignant progression and potentiation of ras-mediated squamous cell carcinogenesis*. *Oncogene*, 2014.
10. Diegelmann, R.F. and M.C. Evans, *Wound healing: an overview of acute, fibrotic and delayed healing*. *Front Biosci*, 2004. **9**: p. 283-9.
11. Wynn, T.A., *Integrating mechanisms of pulmonary fibrosis*. *J Exp Med*, 2011. **208**(7): p. 1339-50.
12. Borensztajn, K., et al., *Protease-activated receptor-2 induces myofibroblast differentiation and tissue factor up-regulation during bleomycin-induced lung injury: potential role in pulmonary fibrosis*. *Am J Pathol*, 2010. **177**(6): p. 2753-64.
13. Borensztajn, K., M.P. Peppelenbosch, and C.A. Spek, *Factor Xa: at the crossroads between coagulation and signaling in physiology and disease*. *Trends Mol Med*, 2008. **14**(10): p. 429-40.
14. Oberst, M.D., et al., *Characterization of matriptase expression in normal human tissues*. *J Histochem Cytochem*, 2003. **51**(8): p. 1017-25.
15. Marchand-Adam, S., et al., *Defect of pro-hepatocyte growth factor activation by fibroblasts in idiopathic pulmonary fibrosis*. *Am J Respir Crit Care Med*, 2006. **174**(1): p. 58-66.
16. Melboucy-Belkhir, S., et al., *Forkhead Box F1 represses cell growth and inhibits COL1 and ARPC2 expression in lung fibroblasts in vitro*. *Am J Physiol Lung Cell Mol Physiol*, 2014. **307**(11): p. L838-47.
17. List, K., et al., *Autosomal ichthyosis with hypotrichosis syndrome displays low matriptase proteolytic activity and is phenocopied in ST14 hypomorphic mice*. *J Biol Chem*, 2007. **282**(50): p. 36714-23.
18. Buzza, M.S., et al., *Membrane-anchored serine protease matriptase regulates epithelial barrier formation and permeability in the intestine*. *Proc Natl Acad Sci U S A*, 2010. **107**(9): p. 4200-5.
19. Fabre, A., et al., *Modulation of bleomycin-induced lung fibrosis by serotonin receptor antagonists in mice*. *Eur Respir J*, 2008. **32**(2): p. 426-36.

20. Sokolova, E., et al., *Protease-activated receptor-1 in human lung fibroblasts mediates a negative feedback downregulation via prostaglandin E2*. Am J Physiol Lung Cell Mol Physiol, 2005. **288**(5): p. L793-802.
21. Wygrecka, M., et al., *Role of protease-activated receptor-2 in idiopathic pulmonary fibrosis*. Am J Respir Crit Care Med, 2011. **183**(12): p. 1703-14.
22. Lee, S.L., R.B. Dickson, and C.Y. Lin, *Activation of hepatocyte growth factor and urokinase/plasminogen activator by matriptase, an epithelial membrane serine protease*. J Biol Chem, 2000. **275**(47): p. 36720-5.
23. Vogel, L.K., et al., *The ratio of Matriptase/HAI-1 mRNA is higher in colorectal cancer adenomas and carcinomas than corresponding tissue from control individuals*. BMC Cancer, 2006. **6**: p. 176.
24. Fernandez, I.E. and O. Eickelberg, *The impact of TGF-beta on lung fibrosis: from targeting to biomarkers*. Proc Am Thorac Soc, 2012. **9**(3): p. 111-6.
25. Stella, G.M., et al., *Activation of Oncogenic Pathways in Idiopathic Pulmonary Fibrosis*. Transl Oncol, 2014.
26. Lin, K.W., et al., *Protease-activated receptor-2 (PAR-2) is a weak enhancer of mucin secretion by human bronchial epithelial cells in vitro*. Int J Biochem Cell Biol, 2008. **40**(6-7): p. 1379-88.
27. Koo, B.H., et al., *Factor Xa induces mitogenesis of coronary artery smooth muscle cell via activation of PAR-2*. FEBS Lett, 2002. **523**(1-3): p. 85-9.
28. Lohman, R.J., et al., *An antagonist of human protease activated receptor-2 attenuates PAR2 signaling, macrophage activation, mast cell degranulation, and collagen-induced arthritis in rats*. FASEB J, 2012. **26**(7): p. 2877-87.
29. Coote, K., et al., *Camostat attenuates airway epithelial sodium channel function in vivo through the inhibition of a channel-activating protease*. J Pharmacol Exp Ther, 2009. **329**(2): p. 764-74.
30. Yamasaki, Y., et al., *Inhibition of membrane-type serine protease 1/matriptase by natural and synthetic protease inhibitors*. J Nutr Sci Vitaminol (Tokyo), 2003. **49**(1): p. 27-32.
31. Rowe, S.M., et al., *Reduced sodium transport with nasal administration of the prostatic inhibitor camostat in subjects with cystic fibrosis*. Chest, 2013. **144**(1): p. 200-7.
32. Kitagawa, M., et al., *Pharmaceutical development for treating pancreatic diseases*. Pancreas, 1998. **16**(3): p. 427-31.
33. List, K., et al., *Matriptase/MT-SPI is required for postnatal survival, epidermal barrier function, hair follicle development, and thymic homeostasis*. Oncogene, 2002. **21**(23): p. 3765-79.
34. Park, Y.S., et al., *Clinical implication of protease-activated receptor-2 in idiopathic pulmonary fibrosis*. Respir Med, 2013. **107**(2): p. 256-62.
35. Vasakova, M., et al., *IL-4 polymorphisms, HRCT score and lung tissue markers in idiopathic pulmonary fibrosis*. Hum Immunol, 2013. **74**(10): p. 1346-51.
36. Okuno, M., et al., *Prevention of rat hepatic fibrosis by the protease inhibitor, camostat mesilate, via reduced generation of active TGF-beta*. Gastroenterology, 2001. **120**(7): p. 1784-800.
37. Gibo, J., et al., *Camostat mesilate attenuates pancreatic fibrosis via inhibition of monocytes and pancreatic stellate cells activity*. Lab Invest, 2005. **85**(1): p. 75-89.
38. Hayata, M., et al., *Effect of a serine protease inhibitor on the progression of chronic renal failure*. Am J Physiol Renal Physiol, 2012. **303**(8): p. F1126-35.

39. Emori, Y., et al., *Camostat, an oral trypsin inhibitor, reduces pancreatic fibrosis induced by repeated administration of a superoxide dismutase inhibitor in rats*. J Gastroenterol Hepatol, 2005. **20**(6): p. 895-9.
40. Ishikura, H., et al., *The proteinase inhibitor camostat mesilate suppresses pancreatic pain in rodents*. Life Sci, 2007. **80**(21): p. 1999-2004.
41. Morinaga, J., et al., *The antifibrotic effect of a serine protease inhibitor in the kidney*. Am J Physiol Renal Physiol, 2013. **305**(2): p. F173-81.
42. Jia, D., M. Taguchi, and M. Otsuki, *Preventive and therapeutic effects of the protease inhibitor camostat on pancreatic fibrosis and atrophy in CCK-1 receptor-deficient rats*. Pancreas, 2005. **30**(1): p. 54-61.
43. Lareu, R.R., et al., *Essential modification of the Sircol Collagen Assay for the accurate quantification of collagen content in complex protein solutions*. Acta Biomater, 2010. **6**(8): p. 3146-51.
44. List, K., et al., *Deregulated matriptase causes ras-independent multistage carcinogenesis and promotes ras-mediated malignant transformation*. Genes Dev, 2005. **19**(16): p. 1934-50.
45. Harris, J.M., et al., *Cryptogenic fibrosing alveolitis and lung cancer: the BTS study*. Thorax, 2010. **65**(1): p. 70-6.
46. Fries, K.M., et al., *Evidence of fibroblast heterogeneity and the role of fibroblast subpopulations in fibrosis*. Clin Immunol Immunopathol, 1994. **72**(3): p. 283-92.
47. Fernandez, I.E. and O. Eickelberg, *New cellular and molecular mechanisms of lung injury and fibrosis in idiopathic pulmonary fibrosis*. Lancet, 2012. **380**(9842): p. 680-8.
48. Seitz, I., et al., *Membrane-type serine protease-1/matriptase induces interleukin-6 and -8 in endothelial cells by activation of protease-activated receptor-2: potential implications in atherosclerosis*. Arterioscler Thromb Vasc Biol, 2007. **27**(4): p. 769-75.
49. Georgy, S.R., et al., *Proteinase-activated receptor-2 is required for normal osteoblast and osteoclast differentiation during skeletal growth and repair*. Bone, 2012. **50**(3): p. 704-12.
50. Mukai, S., et al., *Matriptase and MET are prominently expressed at the site of bone metastasis in renal cell carcinoma: immunohistochemical analysis*. Hum Cell, 2014.
51. Milner, J.M., et al., *Matriptase is a novel initiator of cartilage matrix degradation in osteoarthritis*. Arthritis Rheum, 2010. **62**(7): p. 1955-66.
52. Barretina, J., et al., *The Cancer Cell Line Encyclopedia enables predictive modelling of anticancer drug sensitivity*. Nature, 2012. **483**(7391): p. 603-7.
53. Knight, V., et al., *Protease-activated receptor 2 promotes experimental liver fibrosis in mice and activates human hepatic stellate cells*. Hepatology, 2012. **55**(3): p. 879-87.
54. Chung, H., et al., *Proteinase-activated receptor-2 transactivation of epidermal growth factor receptor and transforming growth factor-beta receptor signaling pathways contributes to renal fibrosis*. J Biol Chem, 2013. **288**(52): p. 37319-31.

## Figure legends

### Figure 1: Matriptase expression and activity are upregulated in the lungs of IPF patients compared to controls.

(A) Scatter dot plot representation of the mRNA levels of Matriptase assessed in controls (n=22) and IPF (n=29) lung specimens by quantitative reverse transcriptase polymerase chain reaction, and normalized to ubiquitin expression. Results represent the mean fold-increase over control  $\pm$  SEM. \*\* $p < 0.01$ . (B) (Top panel) Immunoblot analysis of Matriptase and PAR-2 expression in lung homogenate of controls (lanes 1-6) or patients (IPF, lanes 8-13). Lane 7: molecular marker. Tubulin serves as loading control. (Bottom panel) Densitometry values for Matriptase and PAR-2 were normalized to tubulin. Values were expressed as fold increase over control (white bars) and are shown in the bar graph. \*\* $p < 0.01$ . (C) The relative proteolytic activity of Matriptase was determined in IPF (n=28) and control (n=26). For each group, the different tissue homogenates were incubated with 100  $\mu$ M of the Matriptase highly selective fluorogenic substrate t-butyloxycarbonyl Boc-Gln-Ala-Arg-MCA (Boc-QAR-AMC) and the fluorogenic release was monitored at 300 minutes. Results presented as mean  $\pm$  SEM are expressed as percentage of fluorescence in control tissues, and are representative of two independent experiments. \*\*\*\* $P < 0.0001$ . (D-F, J) Immunohistochemical Matriptase staining of fibrotic (D-F) or non fibrotic (J) regions of the lung of patients with IPF, showing enhanced Matriptase expression in macrophages and interstitial mononuclear cells (arrows), epithelial cells (arrowhead) overlying a fibroblast focus (FF) (E, inset and F,  $\times 200$ ) and in (myo)fibroblasts of this focus (asterisks). (G, H, I) Representative serial lung sections from the same IPF patients stained for alpha-smooth muscle actin (G), CD45 (H) and ABCA3 (I) staining of the same region. (K) Matriptase isotype control staining. (L) The relative mRNA levels of matriptase were assessed in IPF Type II Alveolar epithelial cells (n=7) and IPF fibroblasts (n=4) by quantitative reverse transcriptase polymerase chain reaction. Results are presented as mean  $\pm$  SEM  $\Delta$ Ct (matriptase -HPRT). \*\*  $P < 0.005$ .

### Figure 2: Differential modulation of Matriptase expression in pulmonary cells.

(A) (Top panel) Western blot analysis of matriptase and PAR-2 expression in primary fibroblasts derived from control (lanes 1-5 and 10-14) or IPF (lanes 6-9 and 15-18), in the indicated conditions (respectively unstimulated, lanes 1-9; or stimulated for 48h with 1ng/mL TGF- $\beta$ ,

lanes 10-18). (Bottom panel) Densitometry values were normalized to GAPDH. Values were expressed as fold changes over control (as indicated in the text) and are shown in the bar graph. \* $p < 0.05$ , \*\* $p < 0.005$ , \*\*\* $p < 0.001$  compared to control (white bars), ## $p < 0.005$  compared to IPF (black bars), \$ $p < 0.05$ , ns: non significant. (B) (Top panel) matriptase immunoblot on cell lysate of NHLF showing that TGF- $\beta$  treatment robustly drives matriptase expression (lane 2) compared to PBS-treated cells (lane 1). (Bottom panel) Densitometry values were normalized to GAPDH. Values were expressed as fold increases over control and are shown in the bar graph \*\*\*\* $p < 0.0001$ . (C) (Top) Effect of different concentrations of Matriptase on its own expression in primary control fibroblasts. Cells were stimulated for 48h with PBS (lane 1) or Matriptase (lanes 2-4). (Bottom). The levels of matriptase in each experiment was normalized to GAPDH. Values of all treated samples were then normalized to that of vehicle treated sample that is set to 1 (dotted lines). ns, not significant. (D) (Top) Western blot analysis of A549 cell lysate showing the effects of PBS (lane 1), 1-5 ng/mL TGF- $\beta$  (lanes 2-3) or 1-10nM Matriptase (lanes 4-5) on Matriptase expression. (Bottom) Densitometry values after normalization to GAPDH, shown as fold change over vehicle treated cells (dotted lines). A-D: GAPDH serves as a loading control.

**Figure 3: Matriptase signals to pulmonary cells via PAR-2 activation and triggers fibroproliferative responses.** (A) (Top) Matriptase-induced phosphorylation of ERK1/2 and Akt in fibroblasts is mediated by PAR-2. Serum-starved control pulmonary fibroblasts were treated with PBS (lane 1), 0.1-10nM of Matriptase for 30 minutes (lanes 2-4), or 1nM Matriptase for 0-60 minutes (lanes 5-8). Lanes 9-10: fibroblasts were preincubated for 30 minutes with the PAR-2 blocking antibody SAM-11 and subsequently stimulated with PBS (lane 9) or 1nM matriptase (lane 10). GAPDH serves as a loading control. (Bottom) Densitometry values for P-ERK (white bars) and P-Akt (black bars) were normalized to GAPDH. Values were expressed as fold changes over vehicle treated cells (dotted-line) and are shown in the bar graph. ns, not significant. \* $p < 0.05$ , \*\* $p < 0.005$ , \$ $p < 0.05$  compared to P-ERK in the 1nM matriptase condition; # $p < 0.05$  compared to P-Akt in the 1nM matriptase condition, ns non significant. (B) (Top) Matriptase also activates phospho-ERK1/2 in A549 cells via PAR-2 activation. Serum-starved A549 cells were stimulated either for 10 min with PBS (lane 1) or 0.1-10 nM matriptase (lanes 2-4), or with SAM-11 (lanes 5-8) and subsequently incubated for 10 minutes with 1 and 10 nM Matriptase (lanes 6 and 8). GAPDH serves as a loading control (Bottom) Densitometry values for P-ERK were normalized to GAPDH. Values were expressed as fold changes over vehicle treated cells (dotted line) and

are shown in the bar graph. ns, not significant. \* $p < 0.05$ , \$ $p < 0.05$  compared to P-ERK in the 1nM matriptase condition; ## $p < 0.05$  compared to P-ERK in the 10nM matriptase condition. **(C)** Matriptase enhances primary fibroblast survival via PAR-2 activation. Survival of control primary fibroblasts seeded in medium containing 1% FCS and treated for 48h with PBS ((-), control condition) or the indicated concentrations of Matriptase (+), in the presence (+) or in the absence (-) of the PAR-2 inhibitor GB-88. **(D)** Survival of A549 cells seeded in 1% FCS-containing medium, stimulated for 48h with PBS, 1 or 10 nM of Matriptase. Results are shown as mean  $\pm$  SEM of four **(C)** or three **(D)** independent experiments performed in sextuplicate. ns: non-significant, \*\*\* $p < 0.001$ . **(E)** Migration of Normal Human Lung fibroblasts towards 1% FCS-containing medium (control), or medium supplemented with 1nM Matriptase, in the absence (-) or in the presence (+) of the PAR-2 antagonist GB-88. Results are shown as the mean  $\pm$  SEM of five experiments. ns: non-significant, \* $p < 0.05$ . **(F)** (Top) Matriptase enhances the expression of  $\alpha$ -SMA, collagen and fibronectin in control primary fibroblasts. Western blot analysis of serum-starved cells treated for 48h with PBS (lane 1), or 1 and 10 nM of Matriptase (lanes 2-3). Shown are representative blots of experiments which were performed independently at least three times. GAPDH serves as a loading control. (Bottom) Densitometry values for  $\alpha$ -SMA (white bars), collagen (grey bars) and fibronectin (black bars) were normalized to GAPDH. Values were expressed as fold changes over vehicle treated cells (dotted line) and are shown in the bar graph. ns, not significant. \* $p < 0.05$ . **(G)** (Top) Matriptase-induced protein synthesis is specific and PAR-2 dependent. Western blot analysis of fibronectin expression in serum-starved cells preincubated for 1h with PBS (lane 1), Camostat mesilate (CM; lane 2), GB-88 (lane 3), and subsequently stimulated for 48h with 1nM Matriptase (lanes 4-6). Shown are representative blots of experiments which were performed independently at least three times. GAPDH serves as a loading control. (Bottom) Densitometry values for vehicle (white bars), camostat mesilate (grey bars), and GB-88 (black bars), in the absence (-matriptase) or in the presence (+matriptase) of 1nM matriptase, were normalized to GAPDH. Values were expressed as fold change over vehicle (black line) and are shown in the bar graph. ns, not significant. \* $p < 0.05$ ; \$ $p < 0.05$  and # $p < 0.05$  for 1nM matriptase in the vehicle condition versus CM+matriptase and GB-88+Matriptase respectively; ns: non significant.

**Figure 4: Matriptase inhibition by Camostat mesilate (CM) affords protection from experimental bleomycin-induced pulmonary fibrosis. (A) (Top)** Matriptase activity in murine lung homogenates, determined by the cleavage of the fluorogenic substrate Boc-QAR-

AMC, 3, 7 and 14 days after saline (white bars, respectively n=3, n=3 and n=6 mice per group) or bleomycin instillation (black bars, respectively n=3, n=5 and n=14 mice per group). Results are presented as mean  $\pm$  SEM percentage of Matriptase activity in the saline treated mice at day 3. ns: non-significant, \*p<0.05, \*\*p<0.005. **(Bottom)** Matriptase expression in murine lung homogenate 14 days after saline (lanes 1-3) or bleomycin (lanes 5-8) instillation. Lane 4: molecular marker. GAPDH serves as a loading control. **(B)** Matriptase activity in lung homogenate 14 days after saline (white bars, n=4 mice), sham (CM only, light grey bars, n=4 mice), bleomycin (black bars, n=10 mice) or bleomycin +CM (dark grey bars, n=7 mice) instillation. Results are presented as mean  $\pm$  SEM percentage of Matriptase activity in saline treated mice. ns: non-significant, \*p<0.05 for bleomycin versus saline-treated mice, § p<0.05 for bleomycin versus bleomycin+CM-treated mice. **(C)** Camostat mesilate treatment alleviates the weight loss induced by bleomycin. Depicted is the mean $\pm$  SEM percentage weight loss of the bleomycin (black bars) or bleomycin+CM (dark grey bars) treated mice (n=18 animals per group), compared to their respective controls at the indicated time points. ns: non-significant, \*p<0.05 for bleomycin versus bleomycin+CM-treated mice. **(D)** Collagen content in lung homogenate 14 days after saline (white bars, n=12 mice), sham (CM only, light grey bars, n=10 mice), bleomycin (black bars, n=8 mice) or bleomycin +CM (dark grey bars, n=9 mice) instillation. The collagen content, determined by Sircol assay, was adjusted for tissue weight. Results are expressed as means  $\pm$  SEM; n =8-12 mice per group. \*\*\*p<0.001 for bleomycin versus saline-treated mice, §§ p<0.005 for bleomycin versus bleomycin+CM-treated mice. ns, non significant. **(E)** Hematoxylin and Eosin staining of lung tissue sections from saline-, sham- (WT and WT+CM, top left and top right panels respectively), bleomycin- and bleomycin+CM- (bottom left and bottom right panels respectively) treated mice. **(F)** Assessment of the severity of pulmonary fibrosis on Ashcroft scale 14 days after saline (white bars), sham (CM only, light grey bars), bleomycin (black bars) or bleomycin +CM (dark grey bars) instillation. Depicted is the mean  $\pm$  SEM histological score, n=3-6 mice per group. ns: non-significant, \*p<0.05 for bleomycin versus saline-treated mice, \$\$p<0.005 for bleomycin +CM versus CM, §§ p<0.005 for bleomycin versus bleomycin+CM-treated mice. **(G)** Fibrosis scoring of the Masson's trichrome staining 14 days after saline (white bars, n=3 mice), sham (CM only, light grey bars, n=5 mice), bleomycin (black bars, n=6 mice) or bleomycin +CM (dark grey bars, n=6 mice) instillation. Depicted is the mean  $\pm$  SEM fibrosis score. ns: non-significant, \*\*p<0.005 for bleomycin versus saline-treated mice, §§§ p<0.001 for bleomycin versus bleomycin+CM-treated mice, \$p<0.005 for bleomycin +CM versus CM. **(H)** Semiquantitative scoring of alpha-actin

staining after saline (white bars), sham (CM only, light grey bars), bleomycin (black bars) or bleomycin +CM (dark grey bars) instillation. Depicted is the mean  $\pm$  SEM fibrosis score (n=5-6 mice per group). ns: non-significant, \*\*\*p<0.001 for bleomycin versus saline-treated mice, §§ p<0.005 for bleomycin versus bleomycin+CM-treated mice, \$p<0.005 for bleomycin +CM versus CM. **(I)** Camostat mesilate reduces TGF- $\beta$  expression and SMad 2 phosphorylation in fibrotic lung. (left panel) mRNA expression of TGF- $\beta$  in the different groups of mice. Expression of mRNA was normalized to B2M. Values are expressed as the mean fold-increase over saline group  $\pm$  SEM (n=4-6 mice per group). Ns, non significant, \*p<0.05 for bleomycin versus saline-treated mice, § p<0.051 for bleomycin versus bleomycin+CM-treated mice (right panel, top) Representative western blot analysis of Smad 2 phosphorylation in lung homogenates from mice treated with saline (lanes 1-2), CM only (lanes 6-7), bleomycin- (lanes 3-5) and bleomycin+CM (lanes 8-10) 14 days after bleomycin instillation. GAPDH serves as a loading control. (Right panel, bottom) Densitometry analysis for Smad 2 phosphorylation (p-Smad 2). The dotted lines represent the mean expression of P-Smad 2 in saline treated mice. Data represent the mean  $\pm$  SEM (n=5-6 mice per group). \*\*P < 0.005 for bleomycin versus saline treated mice; \$ p<0.05 for bleomycin +CM versus CM. ns, not significant. **(J)** Camostat mesilate treatment does not change the inflammatory response to bleomycin challenge. Data represent the mean  $\pm$  SEM of macrophage count in the BALF after saline (white bars, n=3 mice), sham (light grey bars, n=4 mice), bleomycin (black bars, n=9 mice) or bleomycin +CM (dark grey bars, n=7 mice) treatment. \*\*P < 0.005 for bleomycin versus saline treated mice; §§p<0.005 for bleomycin +CM versus CM. ns, not significant.

**Figure 5: Matriptase hypomorphic mice are protected from experimental bleomycin-induced pulmonary fibrosis.**

**(A)** Matriptase mRNA levels in pulmonary tissue of matriptase hypomorph mice (n=10 mice) compared with control littermates (n=7 mice) analyzed by qPCR. Shown is mean $\pm$  SEM. \*\*\*p<0.001. **(B)** Collagen content in lung homogenate 14 days after saline (white bars), or bleomycin (black bars) instillation in control and matriptase hypomorphic mice. The collagen content, determined by Sircol assay, was adjusted for tissue weight. Results are expressed as means  $\pm$  SEM; n =3–11 mice per group. \*p<0.05 for bleomycin versus saline-treated control mice. **(C)** Hematoxylin and Eosin staining of Lung tissue sections of control or hypomorphic mice treated with saline (top panels) or bleomycin (bottom panels) for 14 days. **(D)** Assessment of the severity of pulmonary fibrosis on Ashcroft scale 14 days after saline (white bars), or bleomycin (black bars) instillation. Depicted is the mean  $\pm$  SEM histological score, n

=3–9 mice per group. ns: non-significant, \* $p < 0.05$  for bleomycin versus saline-treated control mice, § $p < 0.05$  for bleomycin-treated control mice versus bleomycin-treated hypomorphic mice, §§ $p < 0.005$  for bleomycin versus saline-treated hypomorphic mice. **(E)** Semiquantitative scoring of alpha-actin staining after saline (white bars), or bleomycin (black bars) instillation in control and hypomorphic mice. Depicted is the mean  $\pm$  SEM fibrosis score,  $n = 3-11$  mice per group. ns: non-significant, \*\* $p < 0.005$  for bleomycin versus saline-treated mice, § $p < 0.05$  for bleomycin-treated control mice versus bleomycin-treated hypomorphic mice, §§ $p < 0.005$  for bleomycin versus saline-treated hypomorphic mice. **(F)** Matriptase genetic down regulation is associated with reduced TGF- $\beta$  expression and Smad 2 phosphorylation. (Left panel) mRNA expression of TGF- $\beta$  in matriptase hypomorphic and control littermates. Expression of mRNA was normalized to B2M. Values are expressed as the mean fold-increase over saline group  $\pm$  SEM ( $n = 5-18$  mice per group). Ns, non significant, \*\* $p < 0.005$  for bleomycin versus saline-treated mice, §§ $p < 0.005$  for bleomycin-treated control mice versus bleomycin-treated hypomorphic mice. (Right panel, top) Representative western blot analysis of Smad 2 phosphorylation in lung homogenates from control (lanes 1-5) and matriptase hypomorphic (lanes 6-10) mice treated with saline (lanes 1-2 and 6-7), or bleomycin (lanes 3-5 and 8-10) for 14 days. GAPDH serves as a loading control. (Right panel, bottom) Densitometry analysis for Smad 2 phosphorylation (p-Smad 2). The dotted lines represent the mean expression of P-Smad 2 in saline treated mice. Data represent the mean  $\pm$  SEM ( $n = 6-9$  mice per group). \*\*\* $P < 0.001$  for bleomycin versus saline treated control mice; §§  $p < 0.005$  for bleomycin-treated control mice versus bleomycin-treated hypomorphic mice; ns: non significant.

Table 1

*Matriptase* and *HAI-1* mRNA levels in normal and affected tissues. The mRNA levels were normalised to Ubiquitin mRNA levels.

|                        | mRNA levels in n=22<br>control tissues (mean, SEM) | mRNA levels in n=29 IPF<br>tissues (mean, SEM) |
|------------------------|--|--|
| Matriptase             | 0.0074 (0.0007)                                    | 0.011 (0.001), p=0.0024                        |
| HAI-1                  | 0.093 (0.006)                                      | 0.12 (0.01), p=0.0418                          |
| Ratio Matriptase/HAI-1 | 0.08 (0.006)                                       | 0.099 (0.007), p=0.046                         |

p value for the comparison of the expression levels in control and IPF tissues

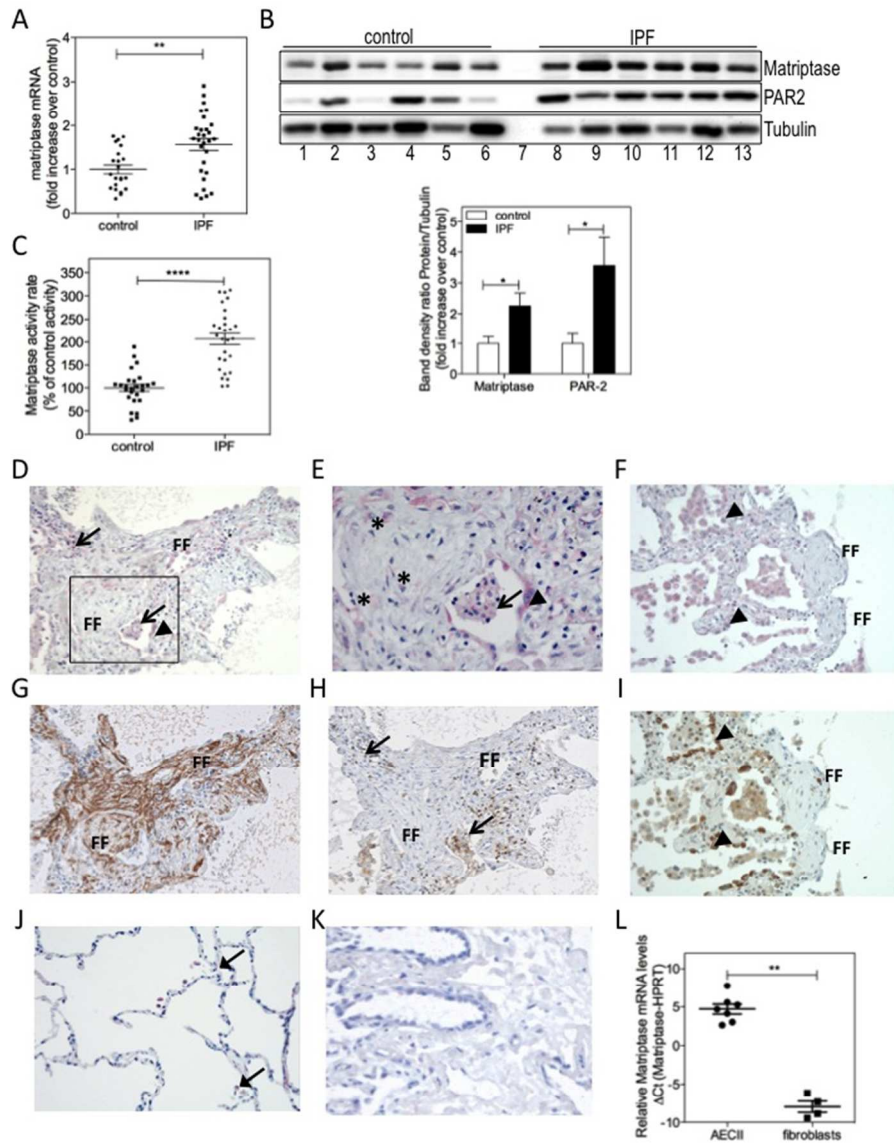


Figure 1  
254x338mm (72 x 72 DPI)

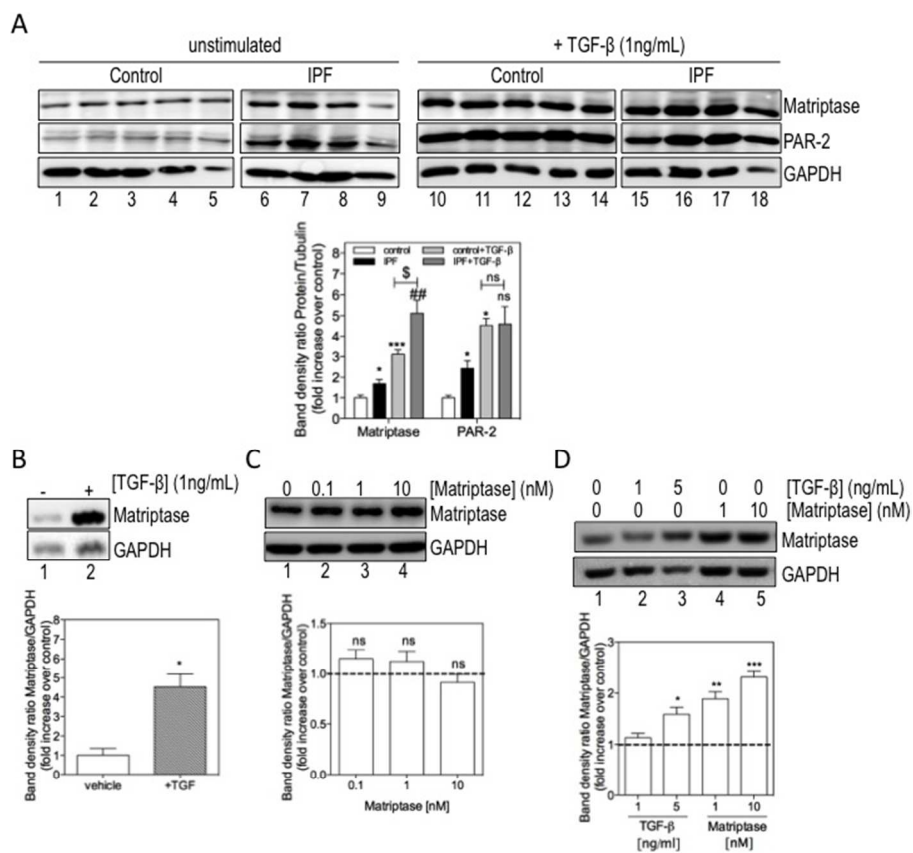


Figure 2  
254x338mm (72 x 72 DPI)

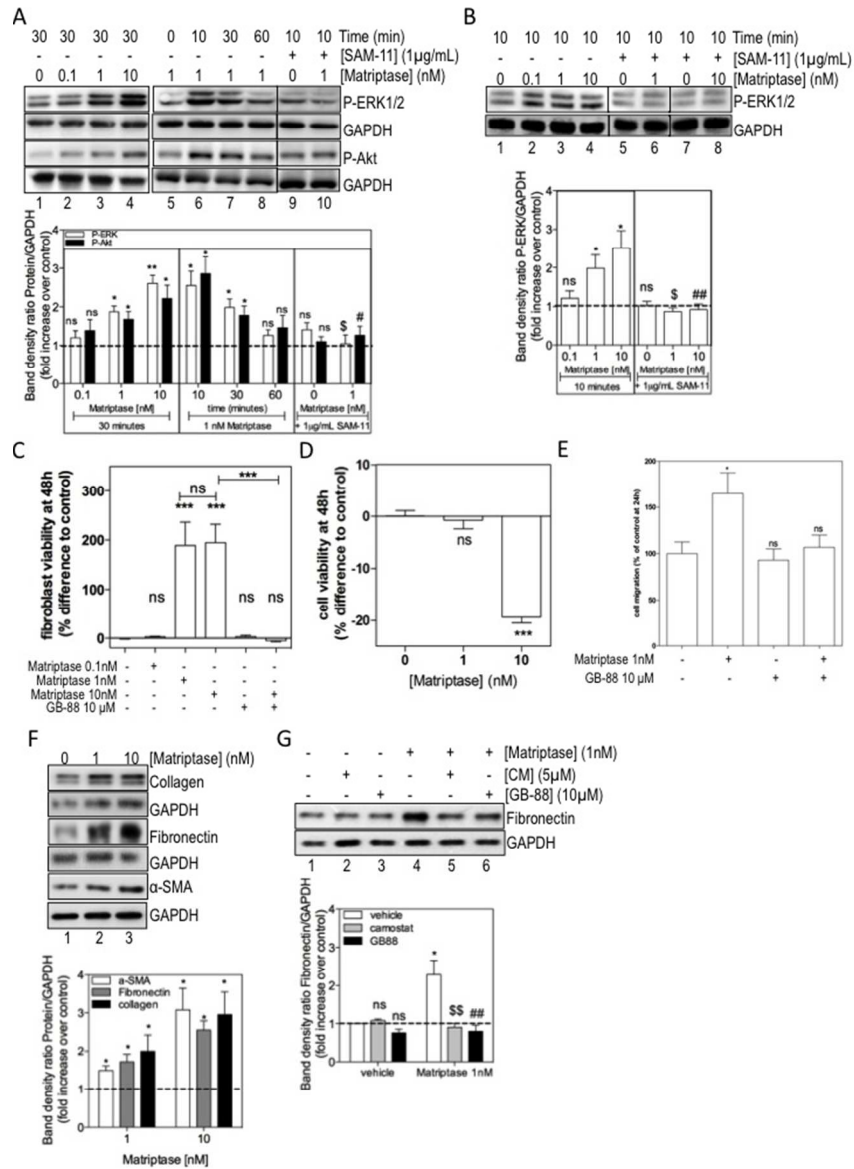


Figure 3  
254x362mm (72 x 72 DPI)

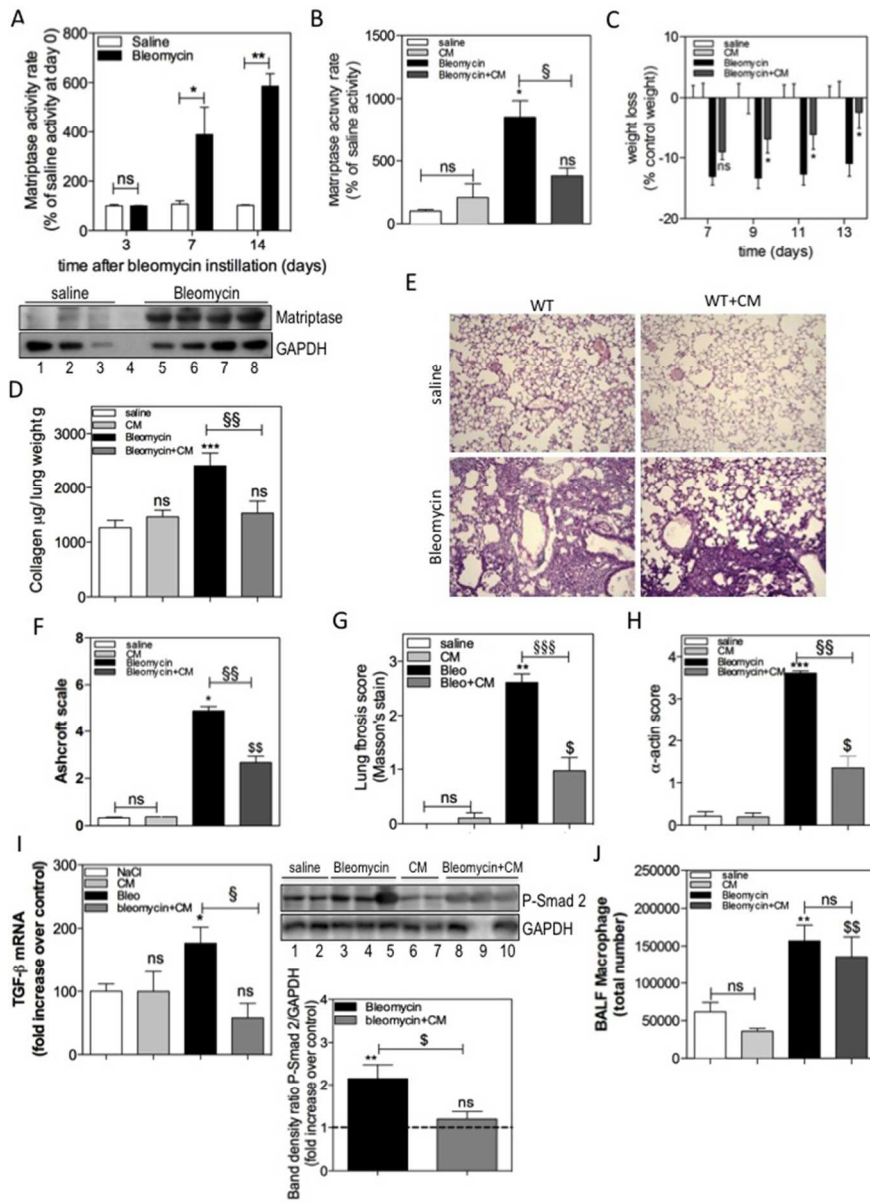


Figure 4  
254x350mm (72 x 72 DPI)

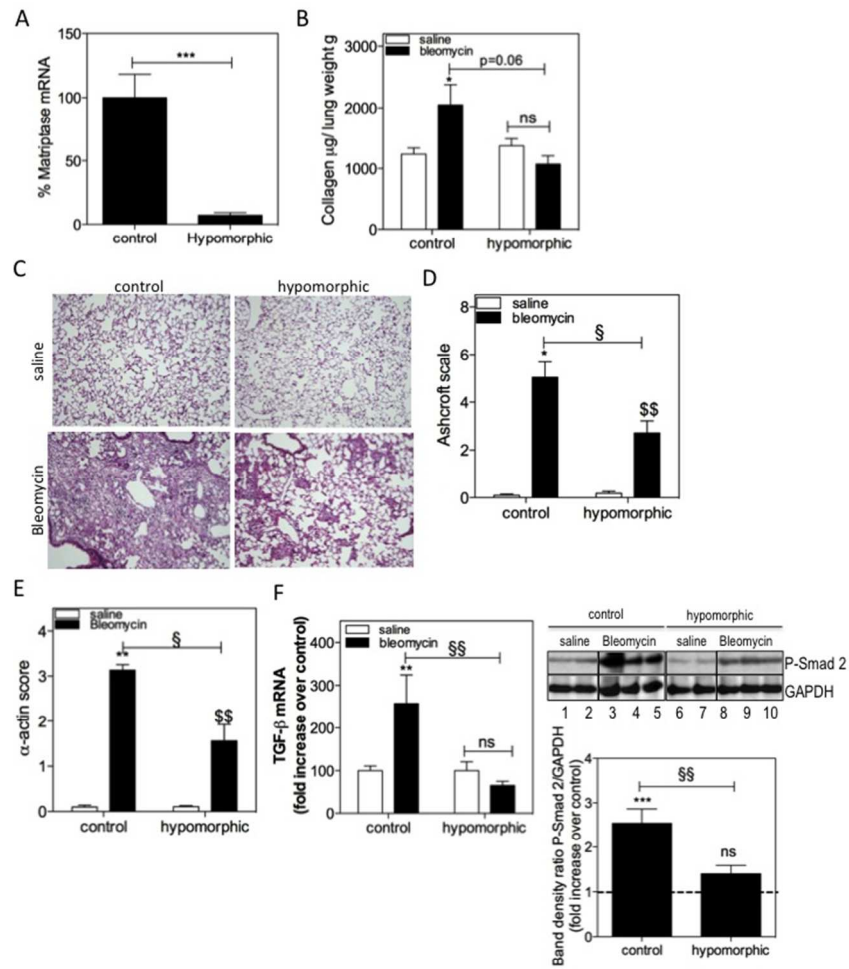


Figure 5  
254x362mm (72 x 72 DPI)

**Membrane-anchored serine protease matriptase is a trigger of pulmonary fibrogenesis****Supplementary information**

**Authors:** Olivier Bardou, Awen Menou, Charlène François, Jan Willem Duitman, Jan H. von der Thüsen, Raphaël Borie, Katiuchia Uzzun Sales, Kathrin Mutze, Yves Castier, Edouard Sage, Ligong Liu, Thomas H. Bugge, David P. Fairlie, Mélanie Königshoff, Bruno Crestani, Keren S. Borensztajn

## Supplemental methods

### Human Tissues

Lung tissue was obtained from 61 patients with IPF (8 females, 53 males; mean age  $57.6 \pm 7.5$  years), and 43 control subjects (patients undergoing lung surgery for removal of a primary lung tumor; mean age  $62.5 \pm 13.8$ , 17 females, 26 males). Control tissues were derived from normal lung sample, obtained from a noninvolved segment, remote from the solitary tumor lesion, as described previously. Normalcy of control lungs was verified histologically (1, 2). Primary fibroblasts were isolated as described in (3). The study protocol was approved by the institutional Ethics committee (comité d'éthique du CEERB Paris Nord, biobank registration number DC 2009-940).

### Isolation of primary IPF human alveolar epithelial cells (phATII) and IPF fibroblasts (German cohort)

Isolation of primary human alveolar epithelial cells was conducted as previously described (4) with some modifications. In brief, tissue specimens were manually minced and digested with a dispase/collagenase mixture (Roche) for 2h at 37°C. Samples were subsequently filtered through nylon meshes and the single cell suspension was centrifuged at 400 g, 4°C for 10 minutes. The cell pellet was resuspended in DMEM/F12 Medium and then layered onto a discontinuous Percoll density gradient (1.04– 1.09 g/ml) and centrifuged at 300 g for 20 minutes. Cells in the interphase representing macrophages and alveolar epithelial cells were recovered and depleted for Macrophages using CD45 specific magnetic beads (Miltenyi Biotec) according to the manufacturer's instructions. Collected cell suspension was centrifuged and the cell pellet was snapped frozen in liquid nitrogen.

### Isolation and culture of primary human lung fibroblasts (phFB)

Isolation of primary human lung fibroblasts was performed as previously described in (5). In brief, human lung tissue was digested using 1mg/ml Collagenase I (Biochrom, Cambridge, UK) for 2 hours at 37 °C. Samples were filtered through nylon meshes to obtain a single cell suspension, which was subsequently centrifuged at 400 g, 4°C for 5 minutes. Cell pellets were resuspended in DMEM/F-12 medium (Life Technologies, Carlsbad, CA, USA) supplemented with 20% fetal bovine serum (Pan Biotech, Aidenbach, Germany) and

Penicillin/Streptomycin (Life Technologies). Cells were cultured on 10 cm cell-culture dishes with a media change at every other day.

### **Antibodies and Reagents**

The following antibodies were used in this study: PAR-2 (SAM11), Matriptase (sc-25234), CD-45 (sc-1178, all from Santa Cruz Technology, Santa Cruz, CA, USA), Matriptase (MAB-3946, R&D Systems, Minneapolis, MN), Fibronectin (ab2413, Abcam, Cambridge, UK),  $\alpha$ -SMA (091m4832, Sigma-Aldrich, St. Louis, MO), Collagen type I (1310-01, Southern Biotech, Birmingham, AL),  $\beta$ -tubulin (ab6046, Abcam, Cambridge, UK), GAPDH (MAB90009, Covalab, Cambridge, UK), ABCA3 (WMAB-ABCA3-13, Seven Hills Bioreagents, Cincinnati, Ohio, USA), phospho-ERK1/2, phospho-Akt and phospho-Smad 2 (#9106s, #9271s and #3101s respectively), all from Cell Signaling Technology (Beverly, MA). The PAR-2 antagonist GB-88 was provided by provided by the University of Queensland (Brisbane, Australia). Camostat mesilate (#3193) was purchased from Tocris (Bristol, UK), and human recombinant protein Matriptase (3946-SE-010) from R&D Systems. Thrombin (T7009;  $\geq 1000$  NIH Units/mg) was from Sigma (Sigma-Aldrich, St. Louis, MO). The different approaches to inhibit matriptase/PAR-2 interactions are summarized in supplemental figure E2.

### **RNA isolation and quantitative reverse transcription polymerase chain reaction.**

Total RNA was extracted using NucleoSpin1 RNA II extraction kit (Macherey Nagel, Hoerd, France) according to the manufacturer's protocol, and cDNAs were generated by reverse transcription using SuperScript II (Invitrogen). To quantify mRNA expression of the indicated genes, quantitative PCR was performed using fluorogenic SYBR Green with specific primers from GenScript and the Sequence Detection System 7700 (Applied Biosystems). Transcripts of Ubiquitin (UBC) for human and Beta2-Microglobulin (B2M) for mouse were used as reference genes in all qRT-PCR reactions. Results were expressed in fold changes compared to control, subsequently to normalization to the reference gene

### **Western Blot**

Samples (cells washed three times with ice cold PBS, or pulverized lungs) were lysed in Laemmli lysis buffer, incubated for 5 minutes at 95°C, and whole lysates were separated by 10% SDS-polyacrylamide gel electrophoresis. After electrophoresis, proteins were transferred to an immobilon-P polyvinylidene difluoride membrane (Millipore, Billerica, MA). Membranes were incubated overnight at 4°C with the indicated primary antibodies. All secondary antibodies were horseradish peroxidase-conjugated from DakoCytomation (Glostrup, Denmark). Blots were imaged using Clarity substrate from Roche (Basel, Switzerland) on an imager Pxi (Syngene, Cambridge, UK). For quantification, densitometry was performed using ImageJ software. Briefly, raw volumes corresponding to the histogram function of the band corresponding to the protein of interest were corrected for those of the loading control. Data are expressed as mean  $\pm$  SEM from (at least) three independent experiments.

### **Immunohistochemistry**

For immunohistochemistry, 4- $\mu$ m (murine) or 5- $\mu$ m (human) sections were first deparaffinized and rehydrated. Heat-induced epitope antigen retrieval was performed using 10 mmol/L citrate buffer pH 6.0, for 40 minutes at 98°C for human matriptase staining. Subsequently, for all stainings, endogenous peroxidase activity was quenched with 0.3% peroxidase blocking reagent (S2023, Dako Denmark, Glostrup, Denmark). anti-aSMA-1 clone 1A4 antibody at 1:4200 (1 hour at room temperature, Sigma-Aldrich, St. Louis, MO), with Histofin mouse stain kit (414322F, Nichirei Biosciences Inc, Tokyo, Japan), using diaminobenzidine staining (K3468, Dako North America Inc, Carpinteria, CA, USA). For human matriptase staining, normal horse serum (S-2000, Vector Laboratories Inc, Burlingame, CA, USA) and BSA 3% were used to block phosphatase activity. Human anti-matriptase primary antibody (Santacruz biotechnology) was used at 1:80 dilution (o/n 4°C), and anti-goat secondary antibody (Vector Laboratories Inc) was applied at 1:300 (30 minutes at room temperature). Phosphatase alkaline stain with Alkaline Phosphatase Standard (AK-5000, Vector Laboratories Inc) and Dako Liquid Permanent Red (K0640, Dako North America Inc) were used to reveal human matriptase. For the isotype control, similar procedures were applied, only the first antibody was omitted. Slides were photographed on a Leica DM4000B with a Leica DFC420 camera (Leica Microsystems GmbH, Wetzlar, Germany).

### **Fluorogenic substrate cleavage assay.**

Matriptase and thrombin activities were evaluated following the hydrolysis of the fluorogenic peptide substrates Boc-QAR-AMC and Boc-VPR-MCA (both R&D systems). Briefly, 10 nM enzyme was mixed with 100  $\mu$ l of peptide substrate (100 $\mu$ M) in a reaction buffer according to the manufacturer's recommendations. The release of fluorescence resulting from hydrolysis of the peptide substrate was monitored on a microplate reader (Varioscan, Thermo Fisher Scientific Inc, Waltham, MA, USA) for 300 min at 37°C with excitation at 360 nm and emission at 480 nm.

### **Cell Culture**

Human pulmonary epithelial cells A549 (CCL-185) were purchased from American Type Culture Collection (ATCC), Rockville, MD. Normal human lung fibroblast (NHLF, CC-2512) were obtained from Lonza (Rockland, ME, USA). Cells were maintained in Dulbecco's modified Eagle's medium or RPMI (A549 cells) supplemented with 10% fetal calf serum and antibiotics, and passed according to routine procedures. Primary pulmonary fibroblasts were used between passage 3-7. Unless stated otherwise, cells were washed twice with PBS, serum-starved 18h and subsequently stimulated as described.

### **Proliferation Assay**

Cells seeded at a density of  $10^4/\text{cm}^2$  in 96-well plates in 100  $\mu$ l DMEM supplemented with 1% FCS, were (if indicated) pretreated with CM (5  $\mu$ mol/L), or PAR-2 antagonist GB-88 (10  $\mu$ mol/L), and subsequently incubated with matriptase, or PBS as a control. Cell proliferation was determined at the indicated intervals using a 2-(4-Iodophenyl)-3-(4-nitrophenyl)-5-(2,4-disulfophenyl)-2H-tetrazolium, monosodium salt (WST-1) assay (Takara, Shiga, Japan), as described in (6, 7).

### **Cell migration**

Cell migration was assayed using a modified Boyden chamber technique (Transwell analysis). 1% serum-containing medium containing PBS as a negative control, 1 nM matriptase, and (if indicated) CM (5  $\mu$ mol/L), or PAR-2 antagonist GB-88 (10  $\mu$ mol/L), was added into the lower chamber as a chemoattractant, and cells ( $5 \times 10^4$ ) were plated in the upper chamber and allowed to migrate for 24 h through 8 $\mu$ m pore filters (Thin Certs-TC inserts, Greiner Bio-one; Brockville, ON). Non-migrating cells were removed from the upper chamber with a cotton swab, filters were stained with Diff-Quik stain, and migrating cells adherent to the underside

of the filter were enumerated using an ocular micrometer and the total number of cells migrated was counted. Data are presented as relative migration compared to control, and represent mean $\pm$ SEM of 4 different experiments.

## **Animals**

C57BL/6N mice were purchased from Janvier Labs (Le Genest Saint Isle, France). When indicated, 0.5 mg camostat mesilate (CM) treatment was initiated 7 days after bleomycin challenge, and administrated intranasally every other day from day 7 until day 14. St14 hypomorphic mice were generated by Pr Thomas Bugge and have been described previously (8-10). Briefly, these mice possess one null allele and one allele in which a reporter gene trap is inserted into the matriptase locus and disrupts gene expression. A low level of alternative splicing in the gene trap allele results in low level synthesis of full length matriptase, which is sufficient to enable mouse survival (9). All experiments performed with St14 hypomorphic mice were littermate controlled from mice generated from heterozygous crosses (8). For all experiments, adult mice (8-10 week-old) received intratracheally bleomycin hydrochloride as previously described (11). Mice referred to as controls received the same volume of sterile phosphate-buffered saline. Mice were sacrificed at the indicated time points after bleomycin challenge. Lung tissues excision for histological analyses, bronchoalveolar lavage (BAL) and BAL cell count was performed as previously described (11). All experiments were performed in compliance with the Institutional Standards for Use of Laboratory Animals.

## **Histopathological Assessment of Pulmonary Fibrosis**

Following fixation, entire mouse lungs were embedded in paraffin. Four-micron thick sections were stained with H&E,  $\alpha$ -actin and Masson's trichrome, according to routine procedures. Different systems were used to assess fibrosis. To prevent observer bias, all histological specimens were randomly numbered and interpreted in a blinded fashion. For each scoring, between 5 and 10 fields in lung lobes (depending on the size and the homogeneity of the histological changes) were examined using light microscopy ( $\times 200$  magnification). Fields were examined to cover each entire lobe and were discarded if nonrepresentative areas or if they included large airways and vessels as described in (12). The mean score for each lobe

was expressed as the average of scores determined in each field. The severity of the lesions was determined by using the Ashcroft scoring system(13). Briefly, each field examined was assessed individually for the severity of fibrotic changes and allotted a score from 0 (normal) to 8 (total fibrosis) using a predetermined scale of severity (numerical fibrotic scale). After examination of the whole section, the mean of the scores from all fields was taken as the fibrotic score. Semi quantitative assessment of  $\alpha$ -actin and Masson's trichrome was performed by grading the stained slides in a blinded fashion as follows:  $\alpha$ -actin was graded on a 0 to 4 scale as follows : 0 = absent staining, 1 = weak staining with focal distribution, 2 = moderate with focal distribution, 3 = strong with focal distribution or weak and diffuse, and 4 = strong and diffuse(14). Masson's trichrome staining was graded on a 0 to 3 as in (15): grade 0, normal lung; grade 1, minimal lesion (lesion area <20%); grade 2, moderate lesion (lesion area, 20–50%); or grade 3, severe lesion (lesion area >50%).

#### **Quantification of secreted collagen**

For quantification of total secreted collagen, the Sircol assay was performed according to manufacturer's instructions (Biocolor, Carrickfergus, UK). The Sircol assay was used without incorporating the recent modified method with a pepsin digestion step described by Lareu and colleagues (16). More specifically, according to the manufacturer's recommendation for soft tissue handling, to minimize background due to the interference of serum proteins - especially albumin in cell culture medium- with the Sircol reagent, the lungs were flushed before excision, then lung samples were further diced and washed in PBS to clear blood

## Supplemental Figure Legends

### **Figure E1: Expression and activity of matriptase in the bronchoalveolar lavage (BAL) of controls and IPF**

(A) Immunoblot analysis of Matriptase expression in (BAL) of controls (lanes 1-4) or patients (IPF, lanes 5-8). (B) Relative proteolytic activity of Matriptase determined in IPF (n=9, black bars) and control (n=7, white bars), as determined by the cleavage of the Matriptase highly selective fluorogenic substrate t-butyloxycarbonyl Boc-Gln-Ala-Arg-MCA (Boc-QAR-AMC) at 300 minutes. Results presented are expressed as percentage of fluorescence in control BALs, and represent the mean  $\pm$  SEM of two independent experiments. \*P<0.05.

### **Figure E2: Summary of the approaches used in the present study to inhibit Matriptase/PAR2 interactions in vitro and/or in vivo.**

**Figure E3: Effect of camostat mesilate on the enzymatic activity of matriptase and thrombin.** (A) Recombinant human Matriptase (10nM) was incubated with 0-10  $\mu$ M camostat mesilate (CM). Subsequently, activity as determined by the cleavage of the fluorogenic substrate Boc-QAR-AMC was measured as described in the Supplemental methods section. Values are representative of an experiment, which was repeated three times. Values are expressed as mean  $\pm$ SEM fold increase over vehicle. Shown is a. \*p<0.05 vs vehicle. Cleavage of the fluorogenic substrates Boc-VPR-AMC (B) and Boc-QAR-AMC (C) by matriptase, or thrombin, in the absence (vehicle, white bars) or in the presence (black bars) of CM. Datas are expressed as mean  $\pm$ SEM RFUs of independent experiments (n $\geq$ 3). \*\*p<0.005, \*\*\*p<0.001 versus Matriptase+vehicle.

## Supplemental References

- E1. Marchand-Adam S, Fabre A, Mailleux AA, Marchal J, Quesnel C, Kataoka H, Aubier M, Dehoux M, Soler P, Crestani B. Defect of pro-hepatocyte growth factor activation by fibroblasts in idiopathic pulmonary fibrosis. *American journal of respiratory and critical care medicine* 2006;174:58-66.
2. Melboucy-Belkhir S, Pradere P, Tadbiri S, Habib S, Bacrot A, Brayer S, Mari B, Besnard V, Mailleux A, Guenther A, Castier Y, Mal H, Crestani B, Plantier L. Forkhead box f1 represses cell growth and inhibits col1 and arpc2 expression in lung fibroblasts in vitro. *American journal of physiology* 2014;307:L838-847.
3. Marchand-Adam S, Marchal J, Cohen M, Soler P, Gerard B, Castier Y, Leseche G, Valeyre D, Mal H, Aubier M, Dehoux M, Crestani B. Defect of hepatocyte growth factor secretion by fibroblasts in idiopathic pulmonary fibrosis. *American journal of respiratory and critical care medicine* 2003;168:1156-1161.
4. Konigshoff M, Kramer M, Balsara N, Wilhelm J, Amarie OV, Jahn A, Rose F, Fink L, Seeger W, Schaefer L, Gunther A, Eickelberg O. Wnt1-inducible signaling protein-1 mediates pulmonary fibrosis in mice and is upregulated in humans with idiopathic pulmonary fibrosis. *The Journal of clinical investigation* 2009;119:772-787.
5. Staab-Weijnitz CA, Fernandez IE, Knuppel L, Maul J, Heinzelmann K, Juan-Guardela BM, Hennen E, Preissler G, Winter H, Neurohr C, Hatz R, Lindner M, Behr J, Kaminski N, Eickelberg O. Fk506-binding protein 10 is a potential novel drug target for idiopathic pulmonary fibrosis. *American journal of respiratory and critical care medicine* 2015.
6. Fischer AS, Metzner J, Steinbrink SD, Ulrich S, Angioni C, Geisslinger G, Steinhilber D, Maier TJ. 5-lipoxygenase inhibitors induce potent anti-proliferative and cytotoxic effects in human tumour cells independently of suppression of 5-lipoxygenase activity. *British journal of pharmacology* 2010;161:936-949.
7. Tang W, Su G, Li J, Liao J, Chen S, Huang C, Liu F, Chen Q, Ye Y. Enhanced anti-colorectal cancer effects of carfilzomib combined with cpt-11 via downregulation of nuclear factor-kappab in vitro and in vivo. *International journal of oncology* 2014;45:995-1010.
8. List K, Currie B, Scharschmidt TC, Szabo R, Shireman J, Molinolo A, Cravatt BF, Segre J, Bugge TH. Autosomal ichthyosis with hypotrichosis syndrome displays low matriptase proteolytic activity and is phenocopied in st14 hypomorphic mice. *The Journal of biological chemistry* 2007;282:36714-36723.
9. Buzza MS, Netzel-Arnett S, Shea-Donohue T, Zhao A, Lin CY, List K, Szabo R, Fasano A, Bugge TH, Antalis TM. Membrane-anchored serine protease matriptase regulates epithelial barrier formation and permeability in the intestine. *Proceedings of the National Academy of Sciences of the United States of America* 2010;107:4200-4205.
10. Netzel-Arnett S, Buzza MS, Shea-Donohue T, Desilets A, Leduc R, Fasano A, Bugge TH, Antalis TM. Matriptase protects against experimental colitis and promotes intestinal barrier recovery. *Inflammatory bowel diseases* 2012;18:1303-1314.
11. Fabre A, Marchal-Somme J, Marchand-Adam S, Quesnel C, Borie R, Dehoux M, Ruffie C, Callebert J, Launay JM, Henin D, Soler P, Crestani B. Modulation of bleomycin-induced lung fibrosis by serotonin receptor antagonists in mice. *Eur Respir J* 2008;32:426-436.
12. Borensztajn K, Bresser P, van der Loos C, Bot I, van den Blink B, den Bakker MA, Daalhuisen J, Groot AP, Peppelenbosch MP, von der Thusen JH, Spek CA. Protease-activated receptor-2 induces

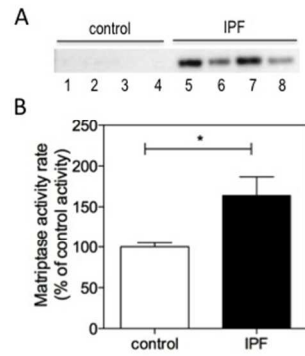
myofibroblast differentiation and tissue factor up-regulation during bleomycin-induced lung injury: Potential role in pulmonary fibrosis. *The American journal of pathology* 2010;177:2753-2764.

13. Ashcroft T, Simpson JM, Timbrell V. Simple method of estimating severity of pulmonary fibrosis on a numerical scale. *Journal of clinical pathology* 1988;41:467-470.

14. Geleilate TJ, Costa RS, Dantas M, Coimbra TM. Alpha-smooth muscle actin and proliferating cell nuclear antigen expression in focal segmental glomerulosclerosis: Functional and structural parameters of renal disease progression. *Brazilian journal of medical and biological research = Revista brasileira de pesquisas medicas e biologicas / Sociedade Brasileira de Biofisica [et al]* 2001;34:985-991.

15. You H, Wei L, Sun WL, Wang L, Yang ZL, Liu Y, Zheng K, Wang Y, Zhang WJ. The green tea extract epigallocatechin-3-gallate inhibits irradiation-induced pulmonary fibrosis in adult rats. *International journal of molecular medicine* 2014;34:92-102.

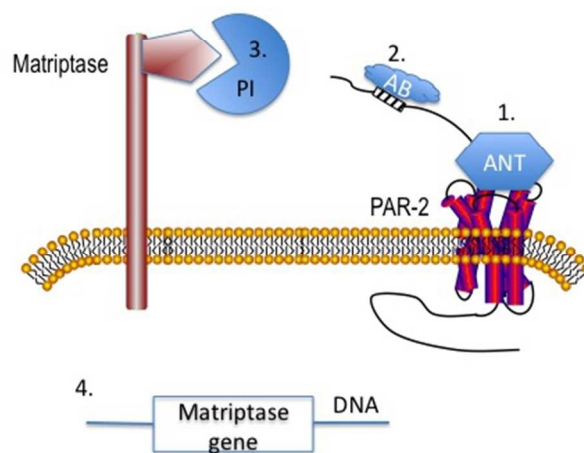
16. Lareu RR, Zeugolis DI, Abu-Rub M, Pandit A, Raghunath M. Essential modification of the sircol collagen assay for the accurate quantification of collagen content in complex protein solutions. *Acta biomaterialia* 2010;6:3146-3151.



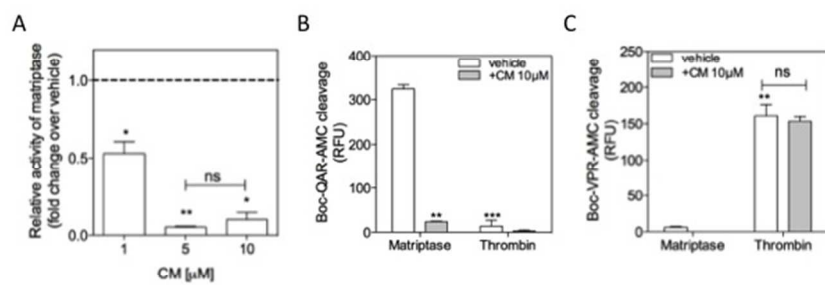
Supplemental Figure E1  
254x362mm (72 x 72 DPI)

**▣ Tethered ligand**

1. Antagonist GB88 (ANT)
2. Blocking antibody SAM11 (AB)
3. Protease inhibitor CM (PI)
4. Genomic approach matriptase gene disruption



Supplemental Figure E2  
254x190mm (72 x 72 DPI)



Supplemental Figure E3  
254x190mm (72 x 72 DPI)